Supplementary Information

The Impact Bimetallic Ni-Fe Deposit Configuration has on Accessing Synergy during Plasma-Catalytic CO_2 Methanation

Ahmad Z. Md Azmi[1], Rachelle Tay[1], Jiajia Zhao[2], Christopher D. Easton[3], Aaron Seeber[3], Yunxia Yang[2], Anthony B. Murphy[4], Emma Lovell[1], * and Jason Scott[1] *

* Corresponding Authors

[1] Particles and Catalysis Research Group, School of Chemical Engineering, UNSW Kensington Sydney NSW 2052

[2] CSIRO Energy, 71 Normanby Road, Clayton South VIC 3168

[3] CSIRO Manufacturing, Private Bag 10, Clayton, VIC 3168

[4] CSIRO Manufacturing, PO Box 218, Lindfield NSW 2070

Table of Contents

List of Figures

List of Tables

1 Catalyst Surface Properties

Table S1: Actual metal loadings of the as-prepared catalysts, and neat Al_2O_3, 10Ni, 10Fe and 10NixFe (where x = 1, 2, 3, 4, 5, 10) Al_2O_3-supported catalysts via ICP-OES Analysis.

	Nominal Loading (wt.%)		WI Loading (wt.%)		DP Loading (wt.%)	
Sample	Ni	Fe	Ni	Fe	Ni	Fe
Al_2O_3	0	0	0	0	0	0
10Ni	10	0	10.6	0	9.6	0
10Ni1Fe	10	1	10.5	1.1	9.1	1.0
10Ni2Fe	10	2	9.8	1.9	9.3	1.9
10Ni3Fe	10	3	9.9	3.3	9.2	2.9
10Ni4Fe	10	4	9.5	4.3	9.5	3.9
10Ni5Fe	10	5	10.1	5.3	9.2	4.8
10Ni10Fe	10	10	8.0	7.8	8.9	9.2
$10Fe/Al_2O_3$	0	10	0	10.5	0	9.7

Table S2: Surface properties of the as prepared catalysts, neat Al_2O_3, and 10Ni, 10Fe and 10NixFe (where x = 1, 2, 3, 4, 5, 10) Al_2O_3-supported catalysts via BET surface area analysis.

	WI			DP		
Sample	S_{BET} (m^2/g)	V_{pore} (cm^3/g)	D_{pore} (nm)	S_{BET} (m^2/g)	V_{pore} (cm^3/g)	D_{pore} (nm)
Al_2O_3	138	0.88	25	165	0.64	15
10Ni	130	0.60	20	139	0.64	17
10Ni1Fe	128	0.58	18	158	0.68	17
10Ni2Fe	125	0.54	17	165	0.68	16
10Ni3Fe	130	0.53	16	168	0.66	16
10Ni4Fe	133	0.56	17	157	0.65	16
10Ni5Fe	139	0.54	15	133	0.60	18
10Ni10Fe	146	0.53	14	153	0.51	13
10Fe	148	0.57	16	164	0.59	14

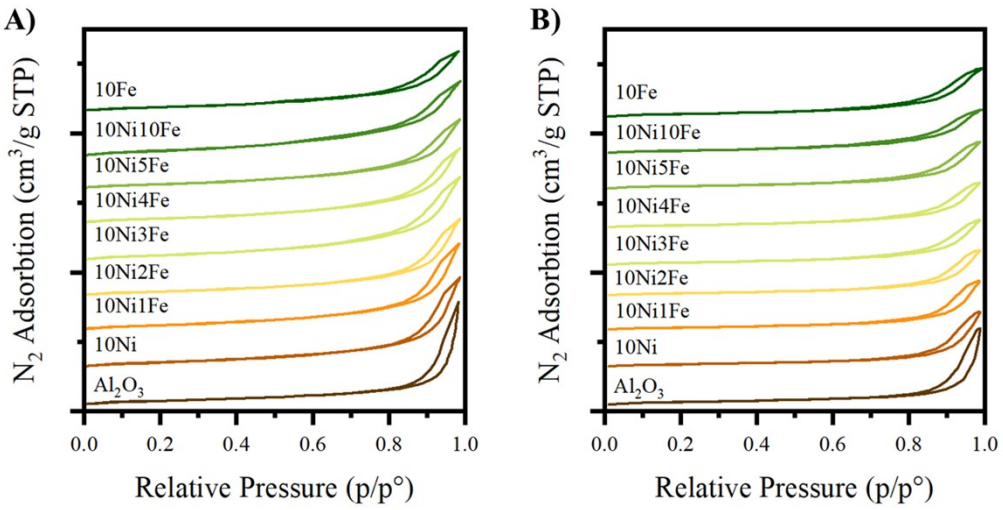

Figure S1: BET N_2 adsorption isotherm plots of the as-prepared catalysts, neat Al_2O_3, and 10Ni, 10Fe and 10NixFe (where x = 1, 2, 3, 4, 5, 10) Al_2O_3-supported catalysts. A) WI, B) DP

2 H_2-TPR Analysis

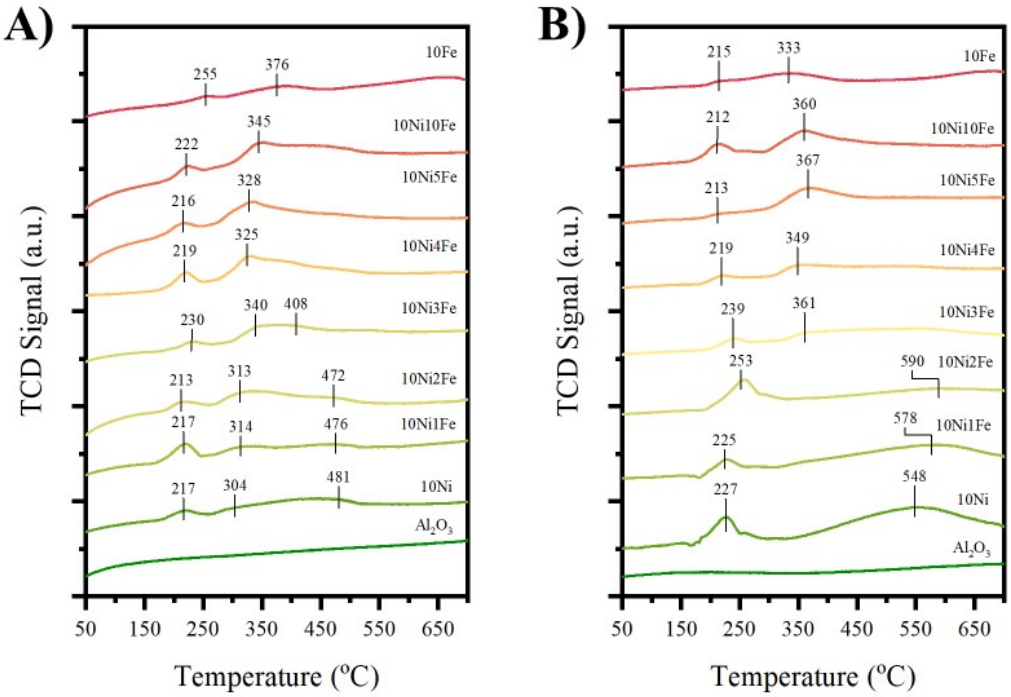

Figure S2: Complete series of H_2-TPR profiles of the as-prepared catalysts, neat Al_2O_3, and 10Ni, 10Fe and 10NixFe (where x = 1, 2, 3, 4, 5, 10) Al_2O_3-supported catalysts. A) WI, B) DP.

3 CO_2-TPDs

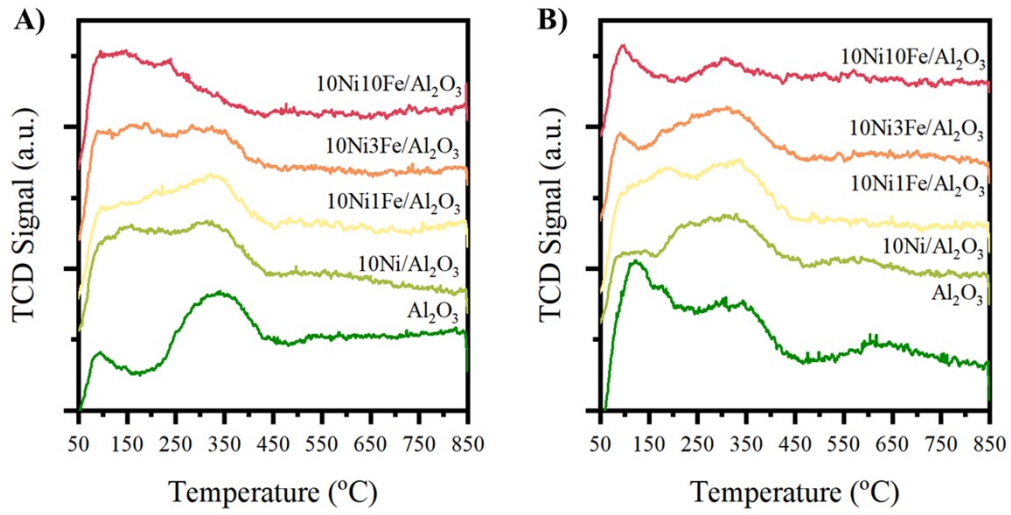

Figure S3: CO_2-TPDs profiles of selected as-prepared catalysts, neat Al_2O_3, and 10Ni and 10NixFe (where x = 1, 3, 10) Al_2O_3-supported catalysts. A) WI, B) DP

4 XRD Analysis

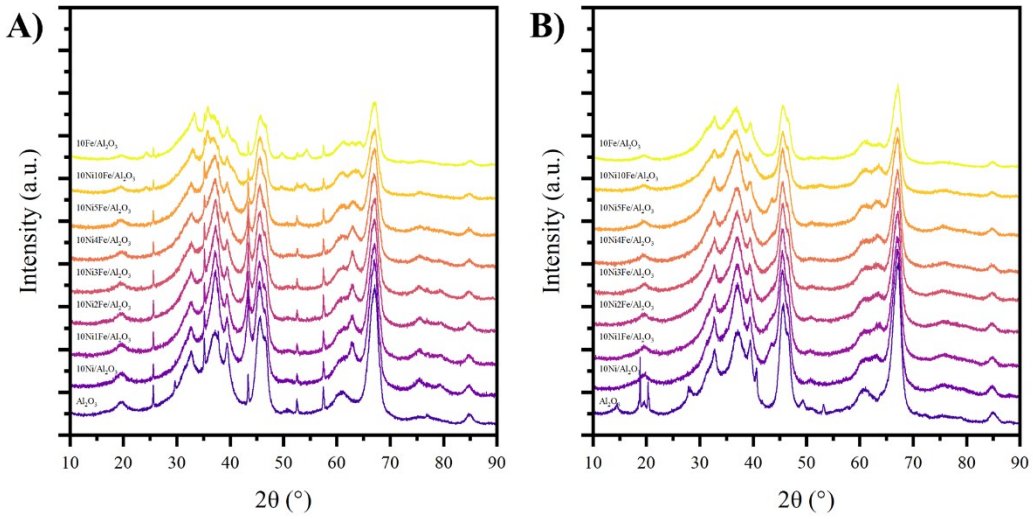

Figure S4: Complete series of XRD diffractograms for the reduced and passivated catalysts, neat Al_2O_3, and 10Ni, 10Fe and 10NixFe (where x = 1, 2, 3, 4, 5, 10) Al_2O_3-supported catalysts. A) WI and B) DP.

5 H_2-TPR, CO_2-TPD and XRD Summary

Table S3: H_2-TPR peak positions, relative H_2 consumption, relative CO_2 desorption and XRD Crystal phases of the as-prepared catalysts 10Ni, 10Fe and 10NixFe (where x = 1, 3, 10) and neat Al_2O_3 for both WI and DP. n.d. denotes not detected and n.t. denotes not tested. Relative H_2 consumption was normalized to $10Ni/Al_2O_3$ WI while Relative CO_2 desorption was normalized to Al_2O_3 WI within their respective temperature ranges.

Sample	H_2-TPR Peak Positions	Relative H_2 Consumption (50-600 °C)	Relative CO_2 Desorption (50-200 °C)	Relative CO_2 Desorption (200-500 °C)	XRD Crystal Phases Identified
$Al_2O_3^{WI}$	n.d.	0	1.0	1.0	n.d.
$10Ni/Al_2O_3^{WI}$	221, 299, 433	1.0	1.9	0.9	NiO
$10Ni1Fe/Al_2O_3^{WI}$	219, 314, 460	0.9	1.8	1.1	NiO
$10Ni3Fe/Al_2O_3^{WI}$	230, 347, 517	1.3	2.2	1.1	NiO
$10Ni10Fe/Al_2O_3^{WI}$	222, 348, 446	2.2	2.2	0.8	Fe_2O_3
$10Fe/Al_2O_3^{WI}$	254, 389, 665	0.6	n.t.	n.t.	Fe_2O_3
$Al_2O_3^{DP}$	n.d.	0	3.1	1.3	n.d.
$10Ni/Al_2O_3^{DP}$	226, 549	1.1	1.4	1.0	NiO
$10Ni1Fe/Al_2O_3^{DP}$	227, 356, 582	1.0	2.1	1.2	NiO
$10Ni3Fe/Al_2O_3^{DP}$	241, 355, 562	0.9	1.6	1.0	NiO
$10Ni10Fe/Al_2O_3^{DP}$	214, 360	1.0	1.4	0.7	n.d.
$10Fe/Al_2O_3^{DP}$	214, 339, 665	0.3	n.t.	n.t.	n.d.

Table S4: H_2-TPR peak positions, relative H_2 consumption, relative CO_2 desorption and XRD crystal phases of the as-prepared catalysts 10Ni, 10Fe and 10NixFe (where x = 1, 3, 10) and neat Al_2O_3 for both WI and DP. n.d. denotes not detected and n.t. denotes not tested. Relative H_2 consumption was normalized to 10Ni/Al_2O_3 WI while relative CO_2 desorption was normalized to Al_2O_3 WI within their respective temperature ranges.

Sample	H_2-TPR Peak Positions	Relative H_2 Consumption (50-600 °C)	Relative CO_2 Desorption (50-200 °C)	Relative CO_2 Desorption (200-500 °C)	XRD Crystal Phases Identified
$Al_2O_3^{WI}$	n.d.	0	1.0	1.0	n.d.
10Ni/$Al_2O_3^{WI}$	221, 299, 433	1.0	1.9	0.9	NiO
10Ni1Fe/$Al_2O_3^{WI}$	219, 314, 460	0.9	1.8	1.1	NiO
10Ni3Fe/$Al_2O_3^{WI}$	230, 347, 517	1.3	2.2	1.1	NiO
10Ni10Fe/$Al_2O_3^{WI}$	222, 348, 446	2.2	2.2	0.8	Fe_2O_3
10Fe/$Al_2O_3^{WI}$	254, 389, 665	0.6	n.t.	n.t.	Fe_2O_3
$Al_2O_3^{DP}$	n.d.	0	3.1	1.3	n.d.
10Ni/$Al_2O_3^{DP}$	226, 549	1.1	1.4	1.0	NiO
10Ni1Fe/$Al_2O_3^{DP}$	227, 356, 582	1.0	2.1	1.2	NiO
10Ni3Fe/$Al_2O_3^{DP}$	241, 355, 562	0.9	1.6	1.0	NiO
10Ni10Fe/$Al_2O_3^{DP}$	214, 360	1.0	1.4	0.7	n.d.
10Fe/$Al_2O_3^{DP}$	214, 339, 665	0.3	n.t.	n.t.	n.d.

6 HRTEM Analysis

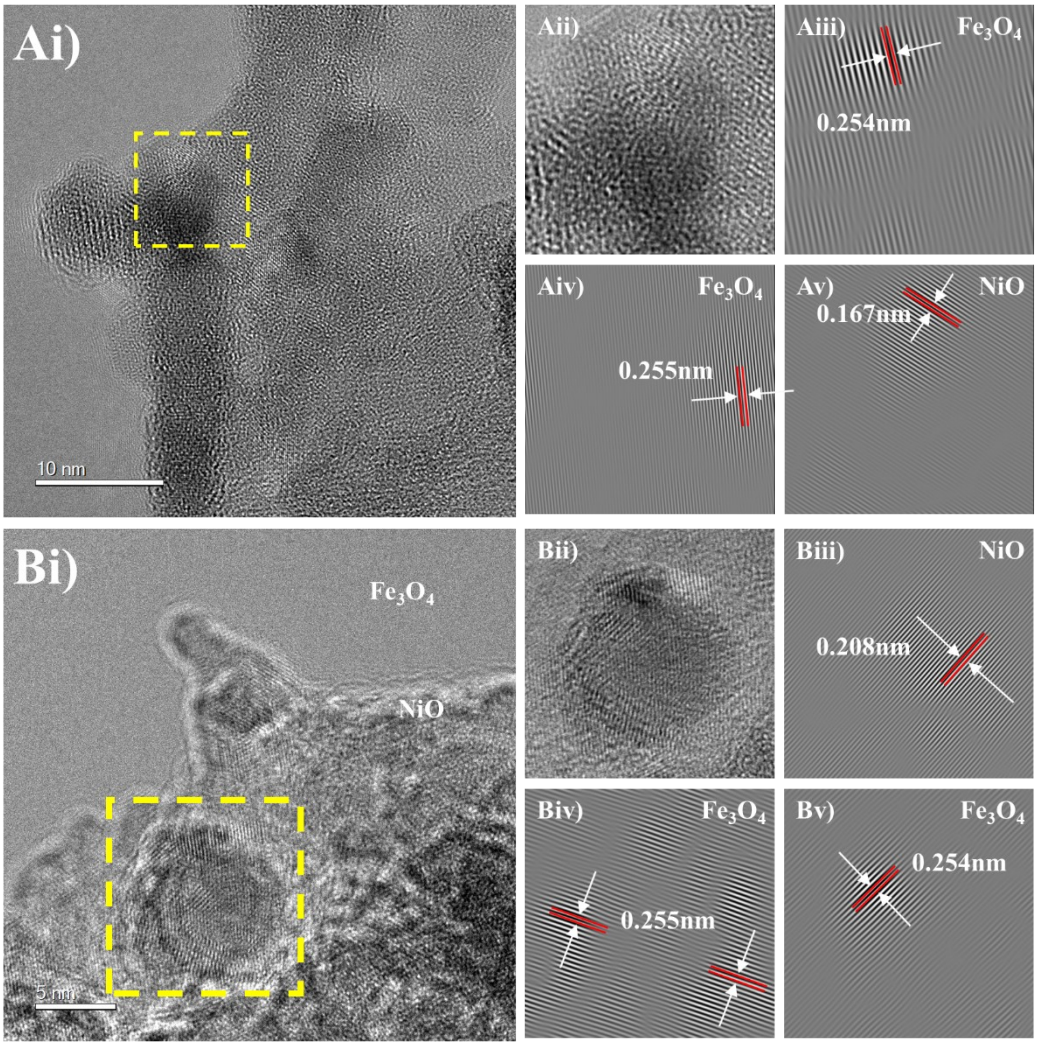

Figure S5: HRTEM micrographs of reduced and passivated 10Ni3Fe/Al_2O_3 catalysts. A) WI, B) WI, i) wide-view micrographs, ii) magnified-view of yellow-dashed highlighted region, iii-v) lattice spacing analysis

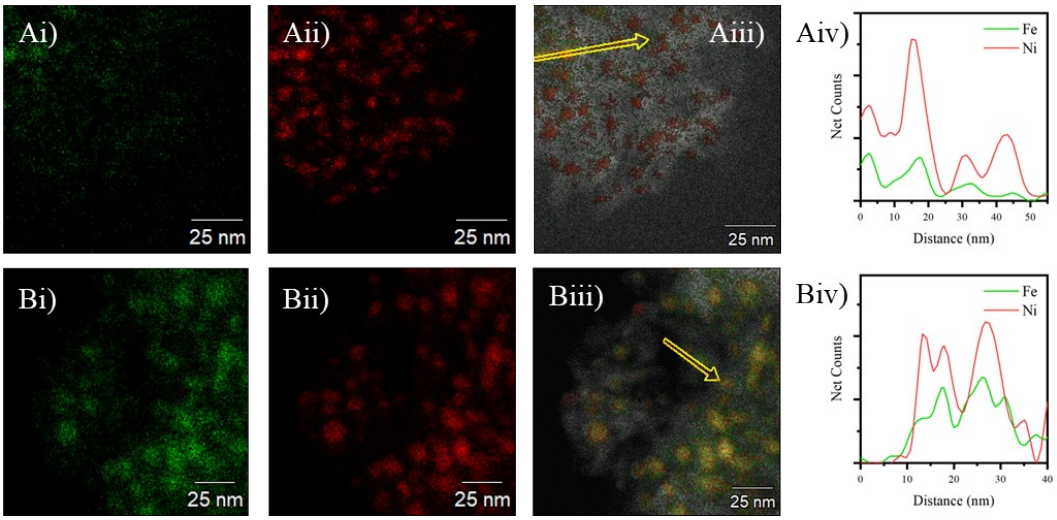

Figure S6: EDS mapping and elemental line scans of reduced and passivated 10Ni3Fe/Al_2O_3 catalysts. A) WI, B) DP; i) Fe mapping, ii) Ni mapping, iii) Ni-Fe mapping overlay, iv) Ni-Fe line scans.

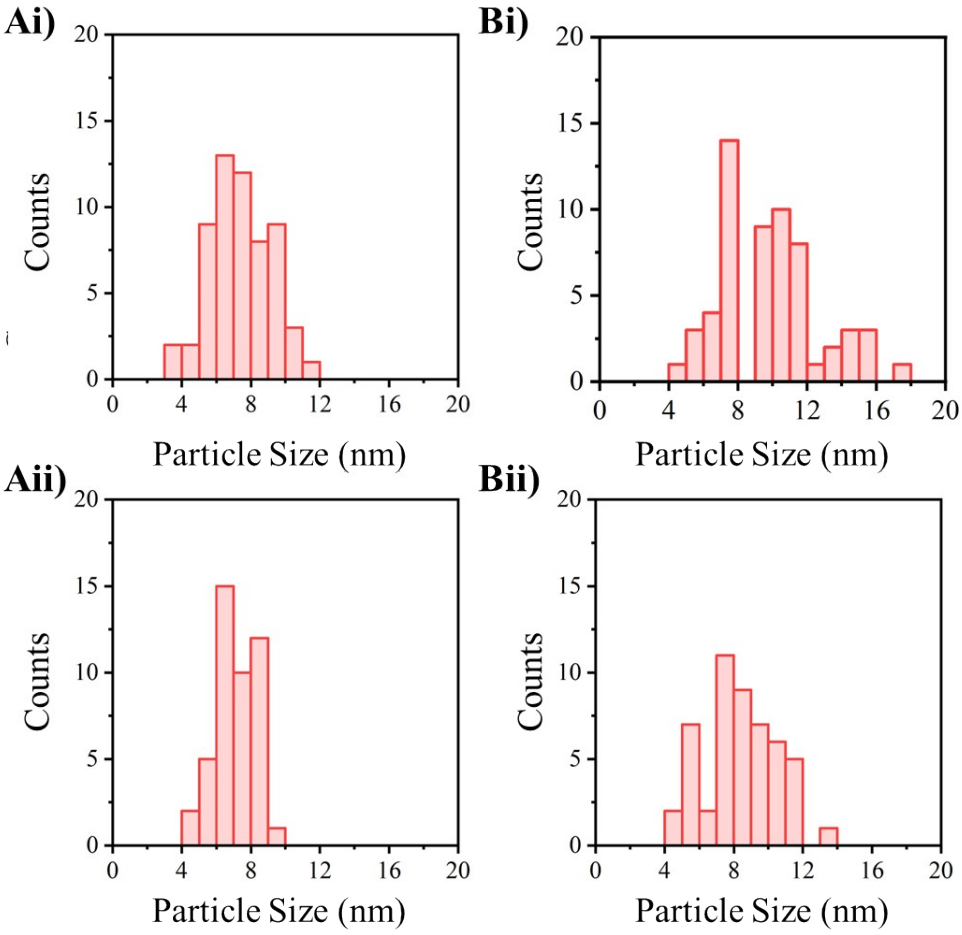

Figure S7: Particle size distribution of the reduced and passivated samples determined through HRTEM micrographs. A) WI, B) DP, i) 10Ni3Fe, ii) 10Ni10Fe

7 XPS Analysis

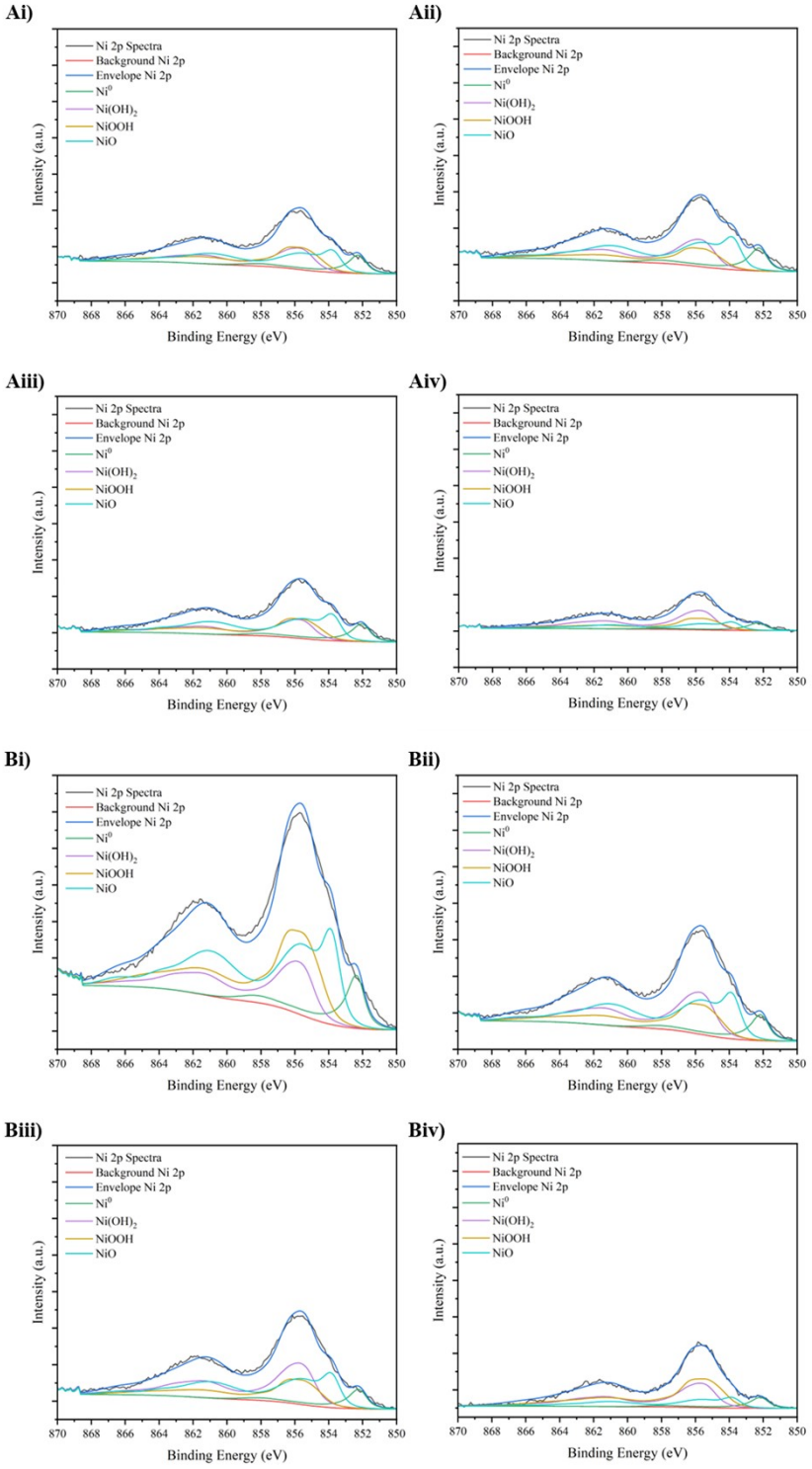

Figure S8: Ni 2p XPS spectra of selected reduced and passivated catalysts, 10Ni and 10NixFe (where x = 1, 3, 10) Al_2O_3-supported catalysts. A) WI, B) DP, i) 10Ni, ii) 10Ni1Fe, iii) 10Ni3Fe, iv) 10Ni10Fe

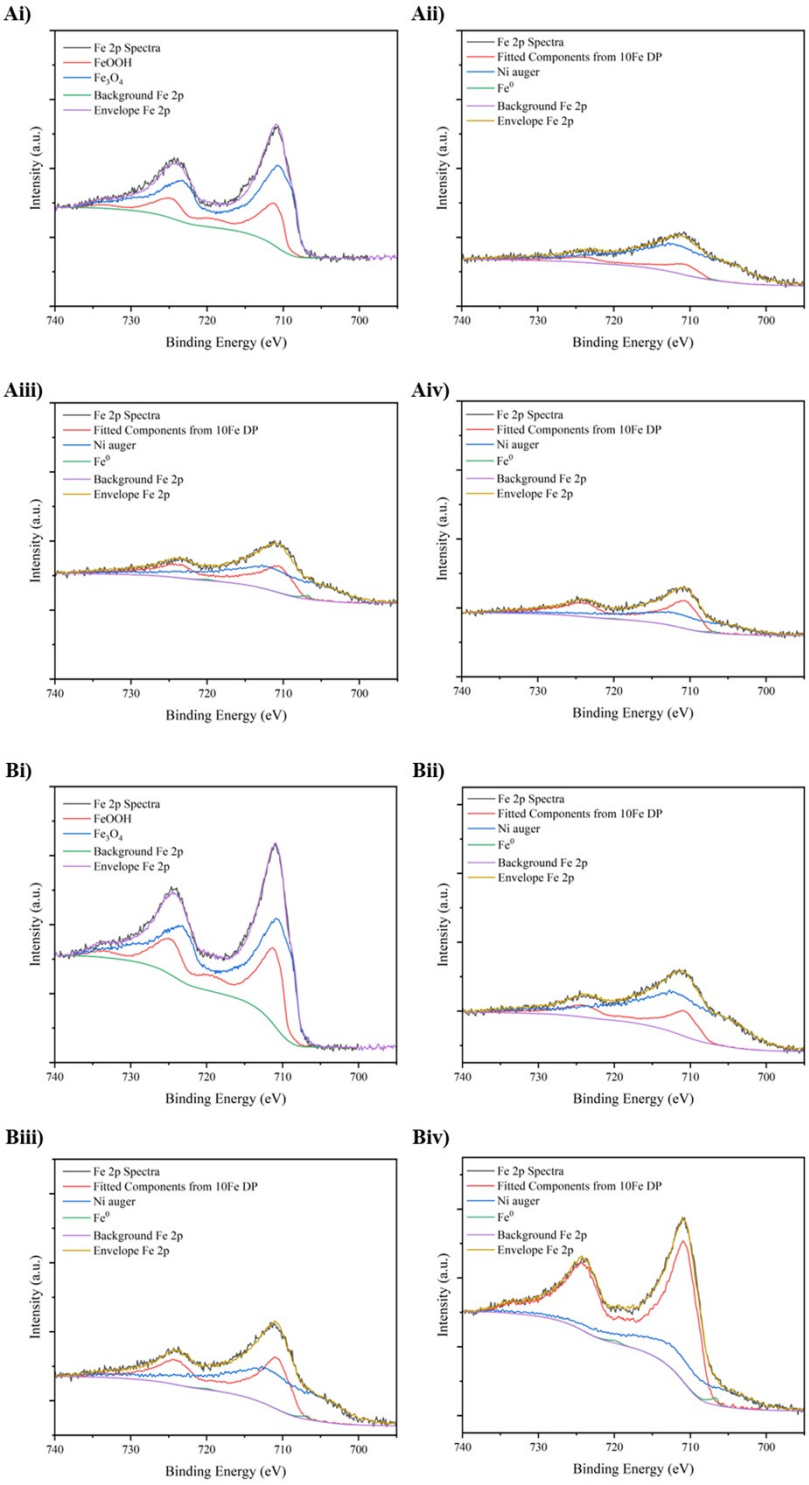

Figure S9: Fe 2p XPS spectra of the reduced and passivated catalysts. 10Fe and 10NixFe (where x = 1, 3, 10) Al_2O_3-supported catalysts. A) WI, B) DP, i) 10Fe, ii) 10Ni1Fe, iii) 10Ni3Fe, iv) 10Ni10Fe

Table S5: Full XPS elemental quantification of selected reduced and passivated catalysts, neat Al_2O_3, 10Ni, 10Fe and 10NixFe (where x = 1, 3, 10) Al_2O_3-supported catalysts for both WI and DP synthesis methods.

	Elemental Atomic Composition (%)								
Sample	F	O	C	Cl	Si	Al	Ni	Fe	Fe/Ni
Al_2O_3 ^{WI}	0.2	55.5	8.8	0.2	0.0	35.3	0.0	0.0	-
10Ni ^{WI}	0.2	53.0	8.7	0.3	0.1	36.4	1.4	0.0	-
10Ni1Fe ^{WI}	0.2	53.7	8.4	0.2	0.4	35.7	1.2	0.1	0.1
10Ni3Fe ^{WI}	0.1	53.6	8.6	0.2	0.1	36.0	1.0	0.3	0.3
10Ni10Fe ^{WI}	0.1	55.0	8.1	0.2	2.0	33.4	0.7	0.5	0.6
10Fe ^{WI}	0.1	55.4	9.6	0.2	0.0	33.4	0.0	1.2	-
Al_2O_3 ^{DP}	0.3	56.2	8.2	0.1	0.2	35.0	0.0	0.0	-
10Ni ^{DP}	0.3	49.6	8.9	0.2	0.0	38.1	2.9	0.0	-
10Ni1Fe ^{DP}	0.2	50.6	10.2	0.2	0.0	36.5	2.0	0.3	0.2
10Ni3Fe ^{DP}	0.3	51.8	9.5	0.2	0.1	35.9	1.7	0.6	0.3
10Ni10Fe ^{DP}	0.3	52.7	10.2	0.2	0.0	33.7	1.1	1.8	1.6
10Fe ^{DP}	0.3	54.6	11.5	0.2	0.0	30.8	0.0	2.6	-

8 Reactor Configuration

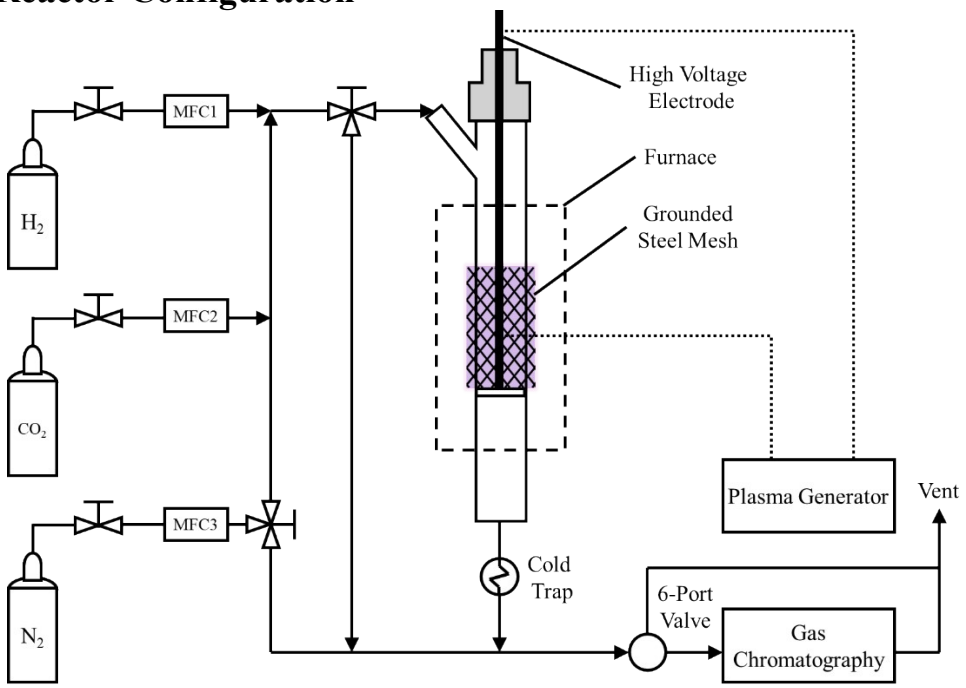

Figure S10: Schematic diagram showing packed-bed DBD reactor for thermal and plasma-thermal CO_2 methanation.

9 Thermal Activity Tests

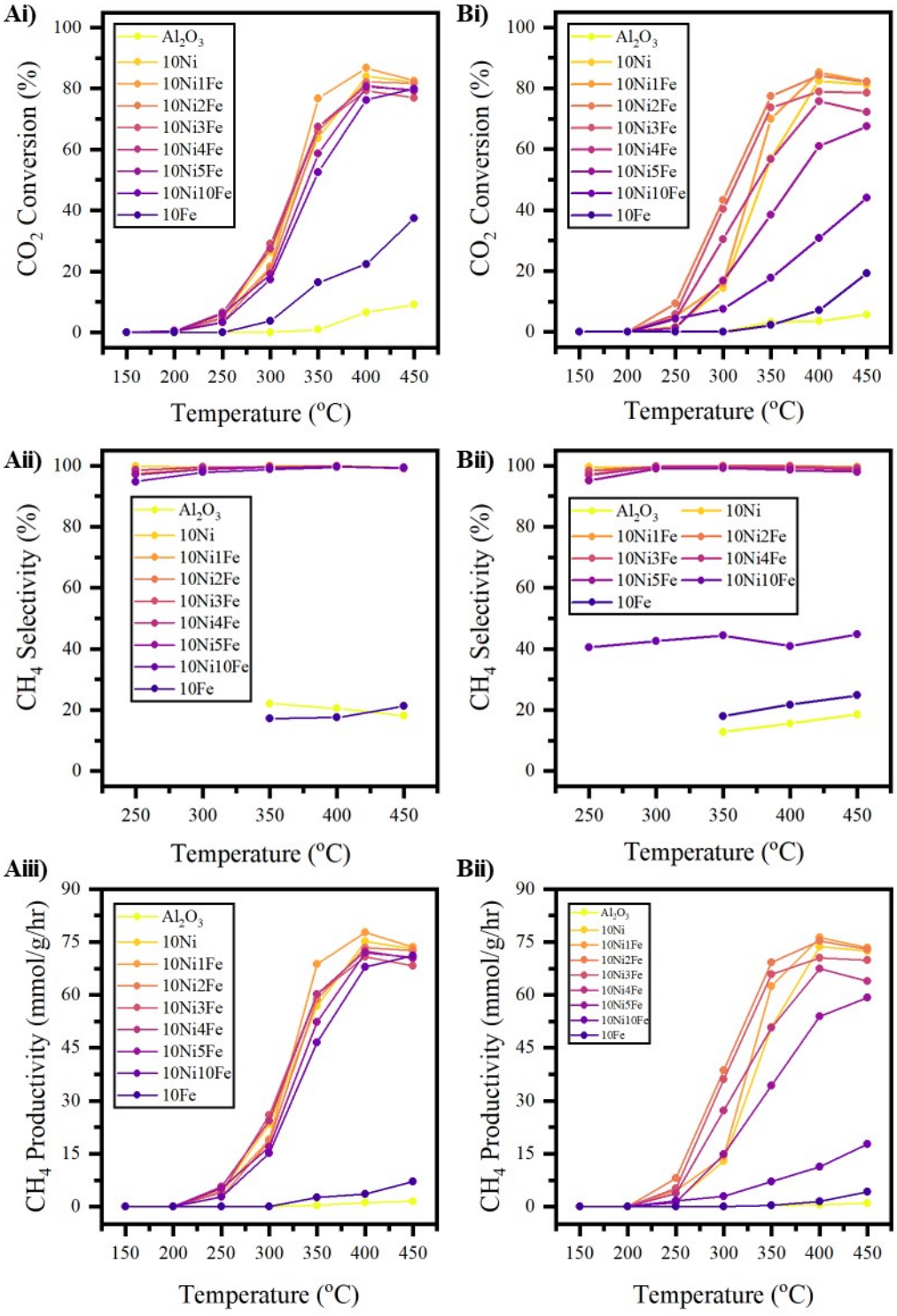

Figure S11: CO_2 conversion and CH_4 selectivity during thermal-catalytic CO_2 methanation by 10Ni, 10Fe and 10NixFe (where x = 1, 2, 3, 4, 5, 10) Al_2O_3-supported catalysts. Neat Al_2O_3 is included as a control. A) WI; B) DP, i) CO_2 conversion, ii) CH_4 selectivity, iii) CH_4 productivity.

10 Plasma Activity Tests

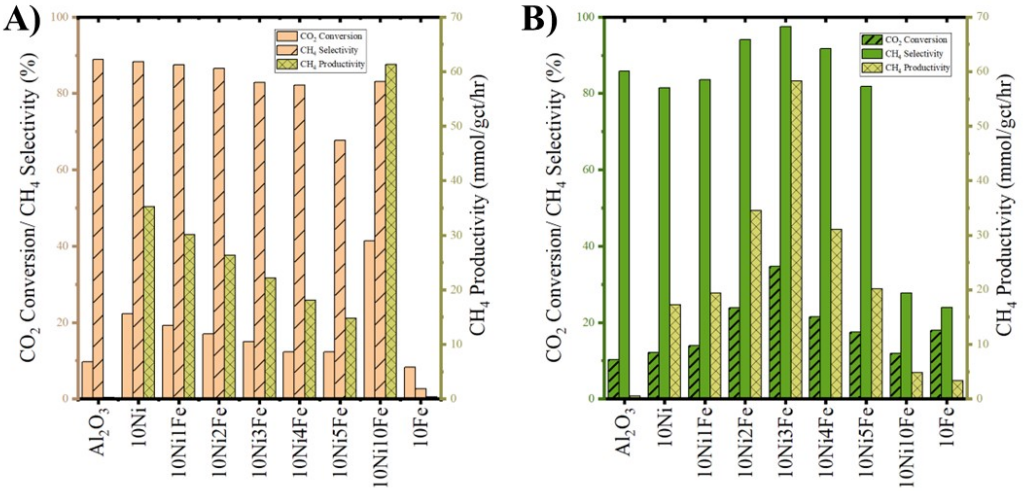

Figure S12: CO_2 conversion and CH_4 selectivity during plasma-catalytic CO_2 methanation by 10Ni, 10Fe and 10NixFe (where x = 1, 2, 3, 4, 5, 10) Al_2O_3-supported catalysts. Neat Al_2O_3 is included as a control. A) WI; B) DP. Operating conditions: voltage = 150 V, discharge frequency = 850 Hz, resonance frequency = 60 kHz, duty cycle = 66 µs, power ~28 W.

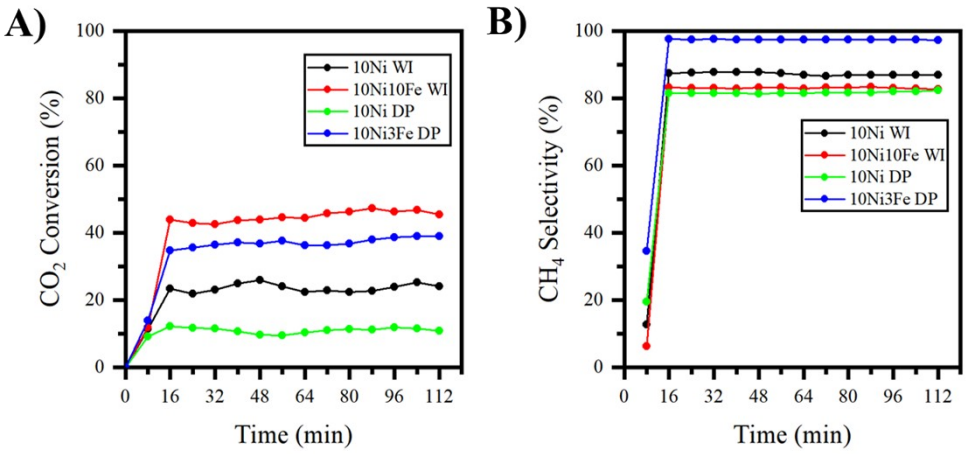

Figure S13: Stability tests of the best performing catalysts (10Ni10Fe/Al_2O_3 WI and 10Ni3Fe/Al_2O_3 DP samples) and monometallic Ni catalysts for both synthesis methods over 2 h at 150 °C in a plasma environment. Voltage = 150 V, discharge frequency = 850 Hz, resonance frequency = 60 Khz, duty cycle = 66 µs, power = ~28 W.

Table S6: Comparison of non-thermal plasma-assisted CO_2 methanation systems of various catalysts, summarizing reactor operating conditions (voltage, frequency, and power) and resulting CO_2 conversion and CH_4 selectivity.

Catalyst	Voltage (kV)	Frequency (Khz)	Power (W)	CO_2 Conversion (%)	CH_4 Selectivity (%)	reference
15Ni/Ce-Zr	10–15	40–41	1–3	77	97	[16]
15Ni/ZSM-5	10	10	14	46.3	88	[36]
15Ni/ Al_2O_3	10	55	15–18	60	97	[27]
15Co/ Al_2O_3	14.6	23.5	2.4	44.6	90	[37]
15Ni/CeO_2	n.s.	7.5–7.7	45	86	86	[38]
$NiFe_{0.1}$/(Mg,Al)O_x-800	9	n.s.	14	84.7	100	[23]
$Ni_{13}Co_2/CaCO_3$	10.8	20	27.8	57.5	92.4	[39]
$NiCo_1/CeO_2$-I	10	7.7	9.9	60	80	[40]
$Ru_{0.5}RH_{0.5}/Al_2O_3$	1-40	20-60	n.s.	97	95	[41]

11 Calculations

Gas flow rates were determined using an internal standard (IS) normalization method. Since the N_2 flow rate was fixed at 10 mL/min, its measured GC peak area was used to correct for variations in injection volume and detector response. The peak areas of all other components (i.e., H_2, CO_2, CO and CH_4) were scaled accordingly based on this reference. The scaling factor was first calculated:

$$SF = \frac{A_{known\ IS}}{A_{measured\ IS}}$$

Where,

SF = Scaling Factor

IS = internal standard / N_2

$A_{known\ IS}$ = known area for IS

$A_{measured\ IS}$ = measured area for IS

The measured areas for the other gas components were scaled using the calculated scaling factor:

$$A_{GC,\ scaled} = S \times A_{GC,measured}$$

Where,

SF = Scaling Factor

$A_{GC,scaled}$ = scaled area of gas component

$A_{GC,measured}$ = measured area of gas component

The gas component flowrates were then calculated using a linear calibration curve of that gas component flowrate vs area.

$$F_{GC} = \frac{A_{GC,scaled}}{CC}$$

Where,

F_{GC} = volumetric flowrate of gas component

$A_{GC,scaled}$ = scaled area of gas component

CC = calibration constant

The calculated flowrates for CO_2, CH_4 and CO were then used to calculate the CO_2 conversion, CH_4 selectivity and CH_4 producitvity.

$$CO_2\ conversion\ (\%) = \frac{CO_{2\ in}\ -\ CO_{2\ out}}{CO_{2in}} \times 100\%$$

Where,

$CO_{2\ in}$ = volumetric flowrate of CO_2 input

$CO_{2\ out}$ = volumetric flowrate of CO_2 output

$$CH_4\ selectivity\ (\%) = \frac{CH_{4\ out}}{CH_{4\ out}\ +\ CO_{out}} \times 100\%$$

Where,

$CH_{4\ out}$ = volumetric flowrate of CH_4 out

$CO_{\ out}$ = volumetric flowrate of CO output

$$CH_4\ productivity\left(\frac{mmol}{ghr}\right) = \frac{CO_2\ conversion\ \times CH_4\ Selectivity \times\ F_{in}\ \times 60}{V_m\ \times\ m_{cat}} \times 100\%$$

Where,

F_{in} = total reactant volumetric flowrate

60 = unit correction for min to hr

V_m = molar volume of gas at STD

m_{cat} = mass catalyst

12 In-Situ OES Analysis

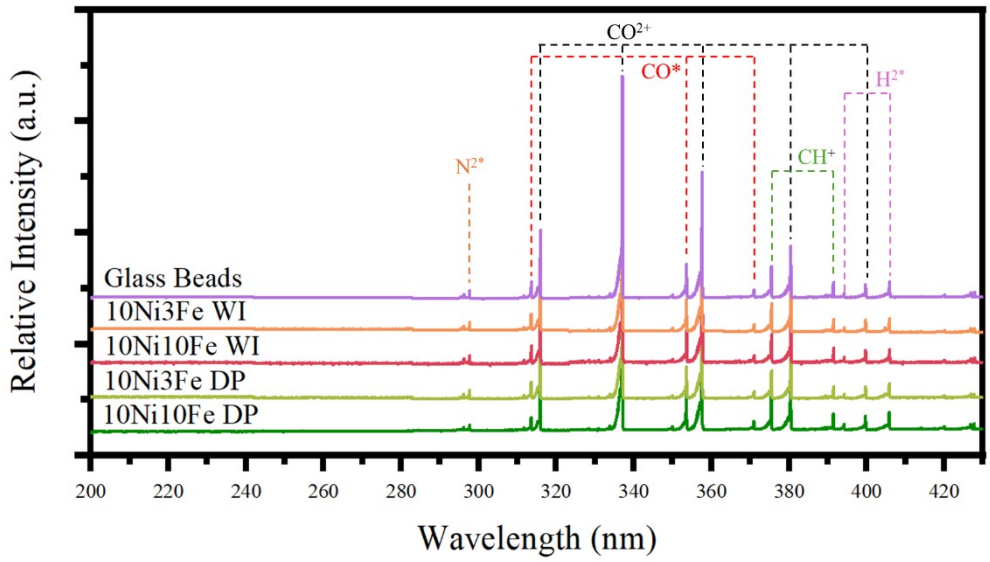

Figure S14: In-situ OES spectra in the range of 200 nm to 430 nm for selected catalysts, 10NixFe (where x = 3, 10) Al_2O_3-supported catalysts for both WI and DP synthesis methods. Glass beads were included as a control.